Baroclinic adjustment and dissipative control of storm tracks

Baroclinic Adjustment and Dissipative Control of Storm Tracks

LENKA NOVAK,[a] MAARTEN H. P. AMBAUM, AND BEN J. HARVEY

Department of Meteorology, University of Reading, Reading, United Kingdom

(Manuscript received 21 July 2017, in final form 11 June 2018)

ABSTRACT

The steady-state response of a midlatitude storm track to large-scale extratropical thermal forcing and eddy friction is investigated in a dry general circulation model with a zonally symmetric forcing. A two-way equilibration is found between the relative responses of the mean baroclinicity and baroclinic eddy intensity, whereby mean baroclinicity responds more strongly to eddy friction whereas eddy intensity responds more strongly to the thermal forcing of baroclinicity. These seemingly counterintuitive responses are reconciled using the steady state of a predator–prey relationship between baroclinicity and eddy intensity. This relationship provides additional support for the well-studied mechanism of baroclinic adjustment in Earth's atmosphere, as well as providing a new mechanism whereby eddy dissipation controls the large-scale thermal structure of a baroclinically unstable atmosphere. It is argued that these two mechanisms of baroclinic adjustment and dissipative control should be used in tandem when considering storm-track equilibration.

1. Introduction

Midlatitude storm tracks are one of the primary drivers of regional and global climate variability, because they redistribute heat, momentum, and moisture. The long-term behavior of storm tracks is highly dependent on diabatic and frictional processes, but this dependency is complex and a major source of climate model biases (Harvey et al. 2013; Zappa et al. 2014, 2015; Pithan et al. 2016). The result is a large uncertainty in climate change predictions, the reduction of which requires better understanding of the underlying dynamics (Shepherd 2014).

Storm tracks are characterized by maxima of baroclinic instability, arising from the radiative imbalance between the pole and equator. Within storm tracks, available potential energy of the mean large-scale flow fuels eddies that in turn modify both the barotropic and baroclinic characteristics of the mean flow. The barotropic characteristics include jet latitude and wind speed, both of which are modified by eddy momentum fluxes. The baroclinic characteristics relate to the thermal properties of the mean flow, such as the mean meridional temperature gradient (which, by thermal wind balance, is proportional to the vertical shear of the mean flow). It is the interaction between the eddies and the baroclinic characteristics of the mean flow that is often seen as the primary control of midlatitude storm tracks (e.g., Pedlosky 1992; James 1994; Novak et al. 2017).

Focusing therefore on this baroclinic eddy–mean flow interaction, Ambaum and Novak (2014) proposed a heuristic model that was later found to reproduce some detailed properties of the temporally oscillating behavior of the North Atlantic and North Pacific storm tracks (Novak et al. 2017). The model is a two-dimensional dynamical system:

$$\frac{ds}{dt} = F - f, \tag{1}$$

$$\frac{df}{dt} = 2f(s - D), \tag{2}$$

where $s = -kdT/dy$ is baroclinicity and $f = kl^2[v^*T^*]$ is meridional eddy heat flux scaled by a constant k and a meridional wavenumber l. Square brackets denote the zonal mean and asterisks the perturbations thereof. Baroclinicity can be viewed as measuring the growth rate of baroclinic eddies and heat flux as measuring storm-track activity (reflecting both eddy density and intensity). The model assumes that the system is mainly forced by a constant thermal forcing of the baroclinicity F and linearly damped by eddy dissipation Df. The assumption of a negligible eddy input and mean output

[a] Current affiliation: California Institute of Technology, Pasadena, California.

Corresponding author: Lenka Novak, lenka@caltech.edu

DOI: 10.1175/JAS-D-17-0210.1

can be justified using observations of global energetics (Oort 1964), where most of the energy input is into the mean available potential energy (proportional to global baroclinicity) and most of the output is via frictional dissipation of eddy energy. The evolution of eddies [Eq. (2)] is derived from the unstable modes of baroclinic instability, where the generating rate by the background baroclinicity is balanced by the dissipation rate of eddies. The reader is referred to Ambaum and Novak (2014) for more a detailed discussion of this model.

The temporal evolution of Eqs. (1) and (2) is analogous to an ecological predator–prey relationship, whereby baroclinicity (prey) is periodically eroded by bursts of eddy heat flux (predator) that mixes temperature horizontally downgradient. This relationship maintains the system in a state that oscillates between being marginally stable and marginally unstable with respect to the intense bursts in storm-track activity (Novak et al. 2017). As Ambaum and Novak (2014) noted, the value of baroclinicity around which the system oscillates between marginal stability and instability is equal to the eddy dissipation constant D in Eq. (2).

In steady state, the Ambaum–Novak model predicts the following two-way equilibration. Baroclinicity is independent of the thermal forcing that replenishes it in the time-varying picture but is proportional to eddy dissipation ($s = D$). On the other hand, steady-state storm-track activity is independent of the eddy dissipation that damps storm tracks in the time-varying picture but is proportional to thermal forcing of large-scale baroclinicity ($f = F$).

Despite the idealized and perhaps counterintuitive nature of the Ambaum–Novak model predictions, existing numerical simulations of the ocean seem to agree with them. For example, in eddy-resolving models of the Southern Ocean, an increase in wind stress (forcing of the mean baroclinicity) has been observed to be associated with insensitivity of the mean baroclinicity but a rapid increase in eddy activity in steady state (Munday et al. 2013). This process is called "eddy saturation." Recent work of Marshall et al. (2017) has also shown that changes in the bottom drag (via which eddy energy dissipates in the time-varying picture) only affect the large-scale baroclinicity in steady state, while eddy energy remains largely unaffected. Thus, Marshall et al. (2017) conclude that their results are consistent with the Ambaum–Novak model predictions except for the limiting cases of vanishing friction and vanishing wind stress.

The atmospheric system is in some ways more complicated than the oceanic one, with the location of eddy generation often coinciding with the location of eddy dissipation, especially in more zonally uniform storm tracks, such as the one over the Southern Ocean. Moreover, the radiative forcing of baroclinicity (as opposed to the wind-driven mechanical forcing in the ocean) may directly result in large changes in static stability throughout the depth of the atmosphere. Additionally, with the atmospheric storm tracks being closely interlinked with the poleward edge of the Hadley cell, global changes in the radiative forcing or friction can provide direct feedbacks from the tropics into the midlatitudes and thus dominate the steady-state responses (e.g., Mbengue and Schneider 2013; Polichtchouk and Shepherd 2016).

Furthermore, a lower thermal expansion coefficient in the oceans has been shown to be associated with different eddy characteristics, such as larger scales of the eddies compared to the deformation scale, reduced eddy diffusivity, and the presence of barotropic inverse cascades (Jansen and Ferrari 2012, 2013). The inverse cascade does not dominate in the midlatitude atmosphere (O'Gorman and Schneider 2007), because of Earth's limited domain size relative to the deformation scale (Zurita-Gotor and Vallis 2009). Baroclinic eddies therefore often interact directly with the mean barotropic flow, in addition to being able to reduce the baroclinicity, and their barotropic feedbacks may substantially intervene with the baroclinic eddy–mean flow interaction.

In spite of these additional complexities, the steady state of Eq. (1) (i.e., $f = F$) has already been shown to hold approximately in the atmosphere. For example, vertical wind shear has been observed to change only by 25% compared to meridional eddy heat flux variability of 280% in response to seasonal changes in radiative thermal forcing (Stone 1978). Additionally, scaling arguments (Stone 1978; Jansen and Ferrari 2013) and GCM studies (Schneider and Walker 2006; Zurita-Gotor and Vallis 2009) have shown that by being able to reduce the vertical wind shear and increase the static stability of the mean flow, eddies can modify the isentropic slope (a measure of the mean baroclinicity) to prevent it from becoming supercritical (steeper than unity), a process called baroclinic adjustment (Stone 1978). It has also been found that, under some parameter settings, the flow can in fact become supercritical, but sensitivity to thermal forcing is relatively low compared to changing other parameters such as the planet size (Jansen and Ferrari 2013; Zurita-Gotor and Vallis 2009). Additionally, for weak enough baroclinicity, static stability change can dominate the eddy-induced baroclinic adjustment, leading to subcritical flows (Schneider and Walker 2006). Nevertheless, the above studies agree that for parameters close to Earthlike values, eddies maintain baroclinicity more or less insensitive to diabatic forcing so that the isentropic slope remains close to unity.

The novel aspect of the steady-state prediction of the Ambaum–Novak model is that the mean thermal wind is controlled by eddy dissipation [i.e., steady state of Eq. (2), $s = D$]. Eddy dissipation represents the combined effect of frictional and diabatic dissipation of eddies as well as their advection out of the domain of interest. On Earth, it is the eddy friction that dominates the total global eddy dissipation (e.g., Oort 1964).

Existing modeling experiments of the atmosphere suggest that the mean flow is sensitive nonmonotonically to surface friction because of opposing effects of eddy and mean friction; baroclinicity increases with increasing eddy friction when the total friction is strong but also increases with increasing mean friction when the total friction is weak (Chen et al. 2007; Zurita-Gotor and Vallis 2009). In addition, Zhang et al. (2012) have found that for sufficiently strong friction, increasing eddy friction increases the meridional temperature gradient while leaving eddy kinetic energy largely unaffected in a quasigeostrophic channel model. These findings suggest that for strong enough friction the Ambaum–Novak argument should work, but this conclusion is not robustly supported or tested in tandem with the baroclinic adjustment mechanism by published studies.

Despite the promising findings above, there are some arguments that are seemingly contradictory to the Ambaum–Novak predictions. For example, Chen et al. (2007) have found strong dependency of storm-track activity to eddy frictional dissipation in a dry GCM, while the predictions above are for eddies and eddy friction to be independent. Furthermore, O'Gorman (2010) and O'Gorman and Schneider (2008) find that in an idealized GCM and in more complex climate models the steady-state mean available potential energy is directly proportional to the thermal mean forcing of the meridional temperature gradient, yet the Ambaum–Novak model prediction is for these to be independent in the steady state.

This paper tests the Ambaum–Novak model predictions in tandem, using a dry intermediate-complexity GCM with a zonally uniform storm track. Using this GCM setup allows the diabatic forcing and eddy friction to be imposed separately while retaining the main realistic features of an Earthlike atmospheric circulation. This would not be possible with complex climate models or observations. In addition, the experiments are implemented in a perpetual equinox so that the GCM can equilibrate and its time mean can be compared to the steady-state predictions of the Ambaum–Novak model. Understanding the sensitivity of baroclinic eddies and mean baroclinicity is of high relevance for understanding storm-track equilibration in changing climates, as well as their sensitivity to drag parameterizations in complex models (e.g., Pithan et al. 2016).

Section 2 describes the model and the setup of the experiments. To test the Ambaum–Novak predictions, section 3 presents responses of baroclinicity and eddy heat fluxes to thermal forcing and eddy friction. Section 4 tests the robustness of these predictions using the responses of the eddy and mean baroclinic energy terms. Section 5 further investigates responses of the isentropic slope and criticality. Section 6 summarizes the findings and discusses them in light of the existing literature.

2. Model setup

The Portable University Model of the Atmosphere (PUMA; Fraedrich et al. 1998) is a dry dynamical core of a global circulation spectral model based on that of Hoskins and Simmons (1975). The setting of 20 equally spaced sigma levels and T42 horizontal resolution (corresponding to 2.815°) was used, since this resolution was found to be sufficient for the study of similar midlatitude dynamics in a similar GCM by Chen et al. (2007). Additionally, PUMA with this resolution was found to produce realistic storm tracks (e.g., Fraedrich et al. 2005), which exhibit the predator–prey-like oscillations in baroclinicity and heat flux that were observed in the North Atlantic and North Pacific (Novak et al. 2017). All experiments were run for 21 years of perpetual equinox. The first spinup year was discarded from the time-mean averages, following Fraedrich et al. (2005).

The diabatic and frictional effects in the GCM are imposed as in Held and Suarez (1994). More specifically, diabatic processes are represented by Newtonian cooling with a time-scale τ_T, and friction is Rayleigh damping of divergence Δ and vorticity ζ with a time-scale τ_F. The model equations are therefore forced as follows:

$$\frac{\partial T}{\partial t} = \cdots - \frac{T - T_r}{\tau_T} - H_T, \tag{3}$$

$$\frac{\partial \zeta, \Delta}{\partial t} = \cdots - \frac{\zeta, \Delta}{\tau_F} - H_{\zeta,\Delta}, \tag{4}$$

where the H terms represent hyperdiffusion that parameterizes subgrid-scale mixing and dissipation. Both the thermal-damping time-scale τ_T and the frictional time-scale τ_F are functions of height, and τ_T is also a function of latitude.

In the control experiment, τ_F is 1 day at the surface and increases to infinity at $\sigma = 0.7$; τ_T is 0.25 days at the equatorial surface and 40 days at the poles and in the upper troposphere. There is no orography, and the pole-to-equator temperature difference of T_r is set to be 60 K,

and T_r is isothermal in the stratosphere. This setup is identical to that in Held and Suarez (1994).

To test the Ambaum–Novak model predictions (i.e., $F = f$ and $s = D$), the equator–pole heating/cooling profile of the GCM was varied in order to simulate changes in F, and eddy friction was varied in order to simulate changes in D. Although diabatic thermal forcing and eddy friction do not exclusively represent the total F and D (which also include advective processes and eddy heating/cooling, both of which are difficult to impose locally externally), they are nevertheless the dominant processes in zonally symmetric storm tracks such as those considered here (e.g., Hoskins and Hodges 2005).

Explorative results (not presented) revealed that imposing eddy friction or thermal forcing globally affects the stratification within the Hadley cell. This tropical response dominates the response in the midlatitude storm-track intensity and latitude, agreeing with the experiments of Polichtchouk and Shepherd (2016) and Mbengue and Schneider (2018). Since responses of the Hadley cell are not the focus of this study, both the thermal forcing and eddy friction changes were limited to higher latitudes with their weighting functions displayed in Fig. 1. Note that the general results are not sensitive to the precise form of these weighting functions as long as the strong tropical response is not triggered.

The thermal forcing was imposed by adding a barotropic tropospheric polar anomaly to the time-invariant temperature field toward which the model is restored [i.e., T_r in Eq. (3)]. Cooling over the polar region increases the large-scale meridional temperature gradient in the T_r field, thus acting as a positive thermal forcing of the large-scale baroclinicity. Centering the temperature anomaly over the poles ensures that the forcing of the baroclinicity is of the same sign everywhere while still forcing the midlatitudes substantially. Since the thermal forcing and the restoration temperature field are zonally symmetric, only the zonal-mean baroclinicity is being forced directly. The ''polar T anomaly'' in the plots below refers to the maximum value of this barotropic temperature anomaly, which is highest over the poles and decreases toward the equator (as shown by the dashed line in Fig. 1).

Note that even though a large part of the heating/cooling is applied outside of the storm-track region, the large-scale temperature gradients that the baroclinic eddies feed on are nevertheless affected substantially. The storm track therefore responds by equilibrating as shown in the following sections. Repeating these experiments with a forcing that extends further into the midlatitudes (not shown) triggers the dominant tropical response discussed above.

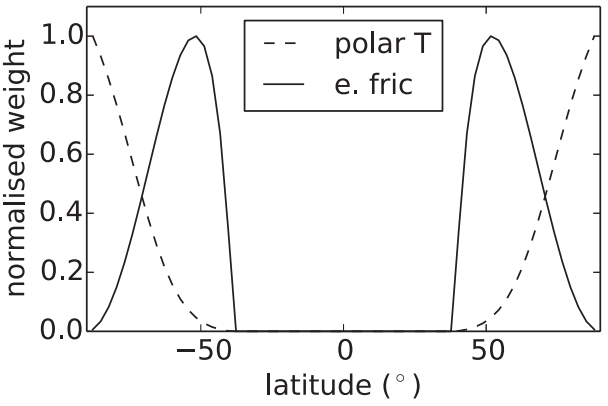

FIG. 1. Meridional structure of the weight applied to the eddy friction time scale w_f and the weight applied to the barotropic temperature anomaly w_T used in the forced experiments. The precise formulation of these weights is not essential, but for the sake of completion, $w_f = \max[0, -(0.05\phi^{-8} + 0.01\phi^2 - 1)(1 - \cos^2 2\phi)]$ and $w_T = \max[0, -(0.1\phi^8 + 1)^{-1} + 1]$. Note that both weights were normalized so that the highest value is one.

In our results below, the forcing is diagnosed as T_R/τ_T, rather than $(T_R - T)/\tau_T$ in order to cleanly isolate the atmospheric adjustment to the external forcing from the external forcing itself. However, the difference between the two ways of characterizing the forcing is quite small since the temperature damping term of the Newtonian cooling responds in such a way that it increases slightly where T_R/τ_T is forced to increase and vice versa. It was found that, for example, a 50–60-K meridional temperature difference in the T_R gradient corresponds to a 20% change in the ''T_R-only forcing'' and 35% in the ''$T_R - T$ forcing.'' The result would be slightly more sensitive responses for the latter forcing, but the conclusions would remain the same.

Following Chen et al. (2007), changes in the frictional time scale τ_F were applied only to zonal wavenumbers larger than zero so as to limit these changes to eddies only. These frictional changes were applied to a band of extratropical latitudes (weights shown by the solid line in Fig. 1). Eddy dissipation can also be simulated in this idealized model setup by changing the thermal relaxation time scale τ_T. However, diabatic eddy processes act as a sink of eddy energy in models with Newtonian cooling parameterizations, whereas in the real world, diabatic eddy processes are generally a source of eddy energy (e.g., Oort 1964). Nevertheless, for the sake of completion, a set of experiments where both the eddy friction and eddy diabatic damping time scales were changed was conducted and yielded qualitatively similar results (not shown). The small sensitivity of the response to the eddy diabatic damping and the ambiguity over the role of eddy diabatic damping in the GCM are the reasons why only the friction-based set of experiments is

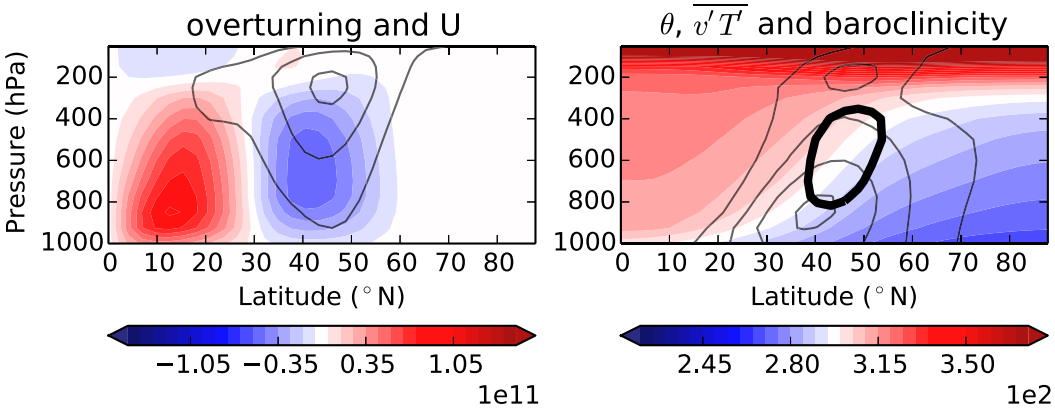

FIG. 2. Control experiment, showing (left) the zonal-mean zonal wind (contours at 10, 20, and 30 m s^{-1}) and the mean meridional overturning circulation (colors; kg s^{-1}) and (right) the potential temperature (colors; K), meridional heat flux (thin contours at showing 5, 10, 15, and 20 K m s^{-1}) and maximum Eady growth rate (thick black contour; 0.5 day^{-1}).

presented below. The "eddy fric. timescale" in the plots below refers to the value of τ_F at the surface in the midlatitudes (where the solid line peaks in Fig. 1).

The results below are from a control run, 19 reference runs (where one of the thermal forcing or eddy friction was being kept at the control value; these runs were used for spatial analysis of the responses), and 70 runs where both thermal forcing and eddy friction were changed (to indicate the robustness of the responses). The polar temperature anomaly range is [−20, −17.5, −15, −12.5, −10, −7.5, −5, −2.5, 0, 2.5, 5, 7.5, 10, 12.5, 15] K and the frictional time-scale range is [0.5, 0.7, 1, 1.3, 1.6, 2] days. Although the thermal forcing and eddy friction changes are imposed in different ways, their ranges were initially selected to have a broadly similar mass-weighted effect. In other words, the friction only operates in the lowest 300 hPa, and the maximum (minimum) values of its range were selected to be a factor of 2 smaller (larger) than in the control run. This is approximately equivalent to the factor of 1.3 for the same damping imposed over the whole tropospheric column (i.e., 800 hPa). This factor was therefore applied to the thermal forcing. The choice of these ranges is justified a posteriori by the similarity of the magnitude of the responses of the global circulation across these ranges (shown in section 2b). Nevertheless, the precise choice of the ranges is not imperative for the results presented below, as it does not affect the relative responses of heat flux and baroclinicity.

a. Control run

The zonal and time averages of temperature, zonal wind, mean overturning circulation, baroclinicity, and eddy heat flux of the control run are displayed in Fig. 2. The heat flux $\overline{[v^*T^*]}$ is computed using the products of the meridional wind and temperature anomalies from the zonal mean, where the square brackets denote zonal mean, the asterisks are the departures from it, and the bar is the time mean. Baroclinicity is diagnosed using the maximum Eady growth rate (EGR), which is a common estimation of the linear growth rate of baroclinic eddies (e.g., Hoskins and Valdes 1990):

$$\mathrm{EGR} = 0.31 f \left[N\right]^{-1} \left[\overline{dU/dZ}\right], \tag{5}$$

where f is the Coriolis parameter, N the static stability, U the zonal wind, Z the geopotential height, and the vertical gradient was calculated using the central difference method. The mean overturning circulation is diagnosed using the mass streamfunction $\left(2\pi a \cos\phi g^{-1} \int_0^p [\overline{v}]\, dp'\right)$.

Figure 2 shows that the control run produces a clear subtropical jet, which has an extended eddy-driven branch reaching lower levels on the poleward side, near the latitude of the maxima of eddy heat flux and baroclinicity. The Hadley and Ferrel overturning cells are also apparent. Since the control parameters were selected to mimic Earth's atmosphere, comparison with the ERA-40 atlas (Kållberg et al. 2005) confirms that the wind and overturning streamfunction patterns and values are comparable to the spring Southern Hemisphere with both the subtropical and eddy-driven jets being present at 30° and 45° latitude, respectively. The subtropical jet is a little weaker in PUMA, and the Hadley cell is weaker in the upper levels, which is expected in a system with no moisture (Kim and Lee 2001). The potential temperature, eddy heat flux, and baroclinicity fields are also comparable to the observed ones (e.g., Kållberg et al. 2005; Novak et al. 2015).

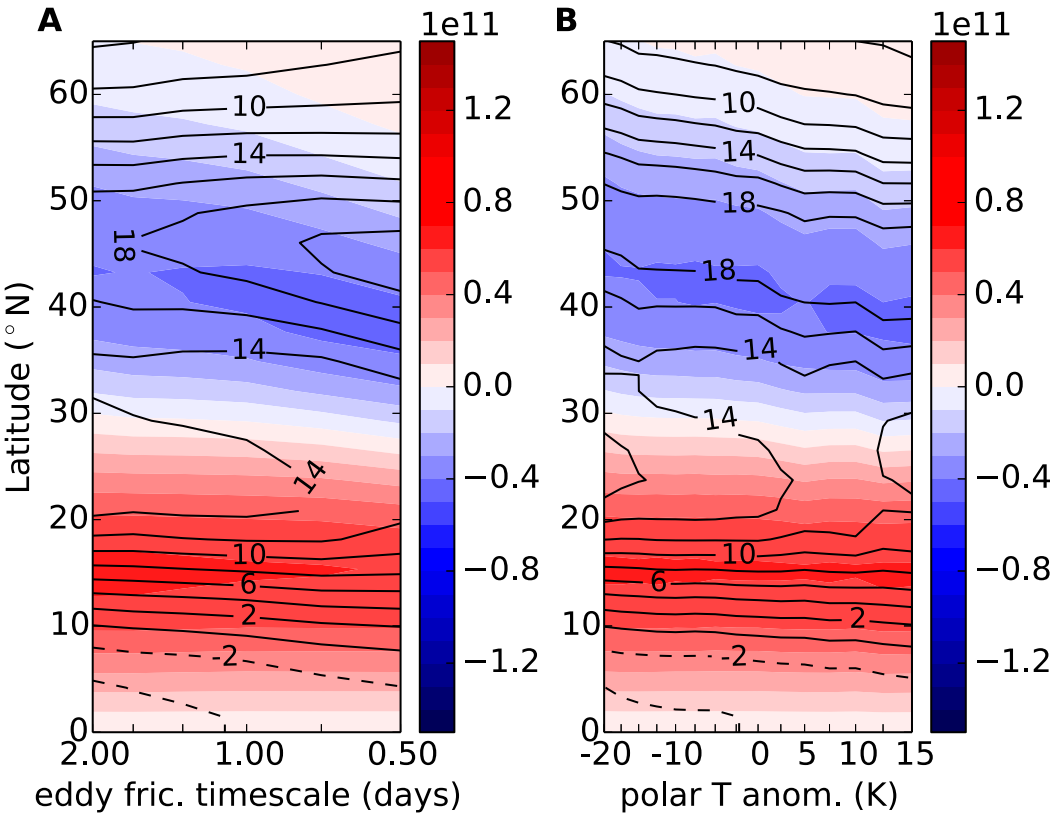

FIG. 3. Mass-weighted average of the overturning streamfunction between 925 and 250 hPa (colors; kg s^{-1}) and thermal wind [black contours; m s^{-2}; defined as the difference between upper-level (250–200 hPa) and low-level (925–700 hPa) zonal wind] for the reference runs when either (a) eddy friction or (b) thermal forcing is changed. Dashed contours mark negative values. The tick marks are placed at values tested by the numerical experiments.

b. Location of circulation response

To check that the response in the equatorward part of the Hadley cell does not dominate the global response, Fig. 3 shows the vertically averaged overturning circulation and thermal wind for the reference runs (i.e., where either eddy friction or thermal forcing is kept constant). The Ferrel cell responds most strongly by shifting in latitude and only slightly in strength. It moves poleward by about 5° with both reduced friction (i.e., increased eddy friction time scales) and increased thermal forcing (i.e., a more negative polar temperature anomaly). This shift is associated with the thermal wind developing a secondary maximum on the poleward flank of the Hadley cell (associated with the subtropical jet) that maintains the Hadley cell fixed equatorward of 30°N. Despite the similar latitudinal shifts in the Ferrel cell for both thermal forcing and eddy friction, the strength of the associated thermal wind maximum that marks the eddy-driven jet is much more sensitive to eddy friction than to the thermal forcing. Because the thermal wind is closely related to baroclinicity, this response is discussed further in the next section.

3. Local baroclinicity and eddy heat flux

Since the Ambaum–Novak predictions are based on the meridional eddy heat flux and baroclinicity, Figs. 4a–d show these two quantities for the reference runs. Baroclinicity and heat flux are computed as in the previous section but here are limited to 775 and 850 hPa, respectively (following Hoskins and Valdes 1990).

Although there is never complete insensitivity to either eddy friction or thermal forcing, it is apparent that heat flux is more sensitive to the thermal forcing whereas baroclinicity is more sensitive to the eddy friction. These responses concur with the Ambaum–Novak prediction.

In accordance with the thermal wind in Fig. 3, Figs. 4e and 4f show that the meridional temperature gradient responses almost mirror the spatial responses in baroclinicity. Conversely, static stability (Figs. 4g,h) mirrors the spatial response of the eddies, which is consistent

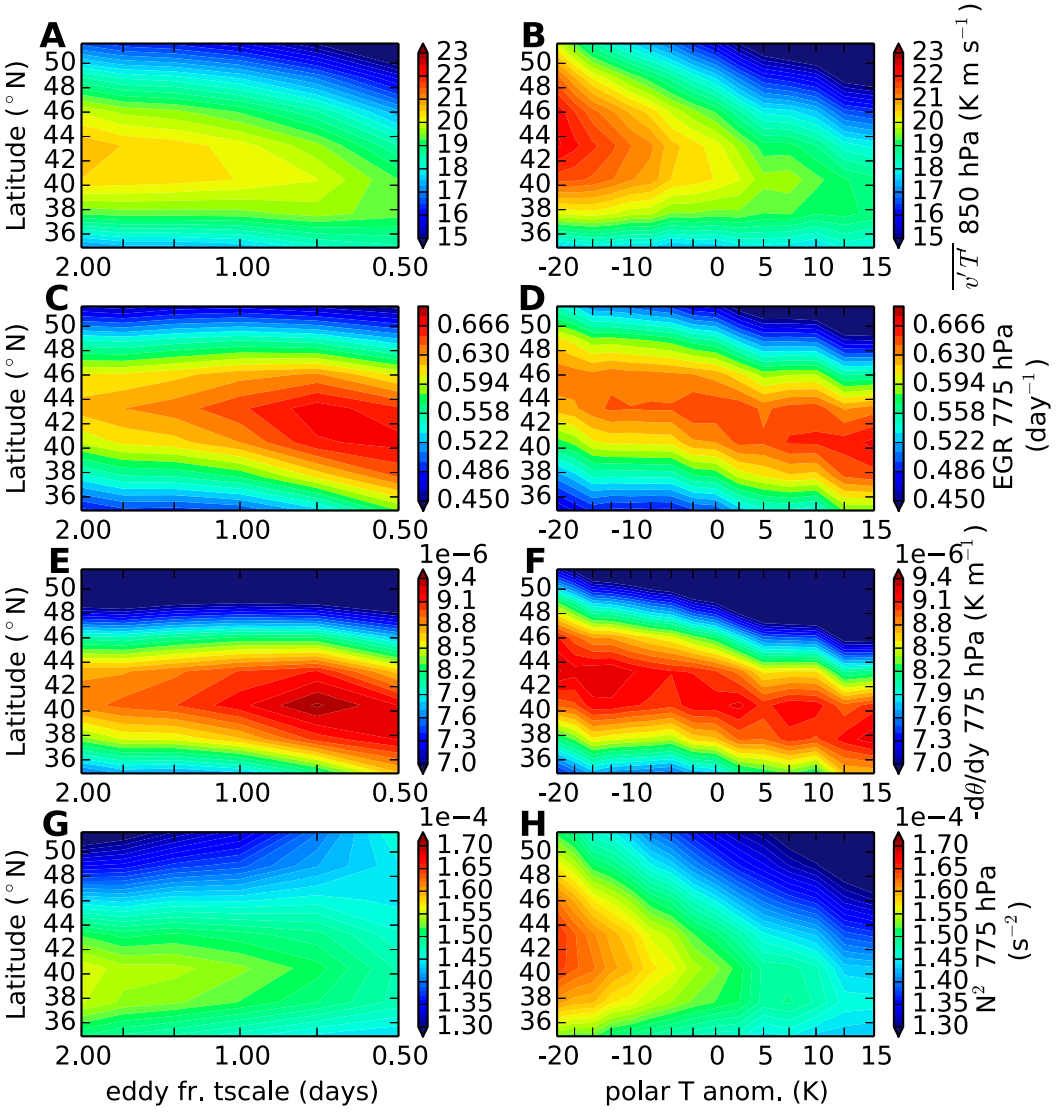

FIG. 4. (a),(b) Low-level heat flux, (c),(d) maximum Eady growth rate, (e),(f) meridional potential temperature gradient, and (g),(h) squared static stability for the reference runs, i.e., experiments where either (left) eddy friction or (right) thermal forcing is varied.

with Schneider and Walker's (2006) observation that eddies stabilize the large-scale flow. For the strongest polar cooling, baroclinicity decreases slightly in intensity even though the vertical wind shear is forced to increase. This is because the response in static stability [N in Eq. (5)] overcompensates slightly for the changes in the vertical wind shear in these cases. This overcompensation has also been observed in GCMs used by Schneider and Walker (2006) and Zurita-Gotor and Vallis (2009).

The rest of this section summarizes results of all forced experiments, where both the eddy friction and thermal forcing were varied. Both low-level zonal-mean baroclinicity and eddy heat flux were averaged over a baroclinic mixing zone in order to isolate the region where eddies are strong enough to drive the baroclinic equilibration [note that this was not necessary in Marshall et al.'s (2017) channel model, where eddy equilibration occurred throughout the whole domain]. This mixing zone is defined as the latitudes where the low-level eddy heat flux is at least 70% of its maximum value, following Schneider and Walker (2008). As opposed to the latter study, the baroclinic zone in the current experiments varies substantially in its meridional extent. This yields results that are not robust for different thresholds of the heat flux percentage. To correct for this, the present study uses the meridional

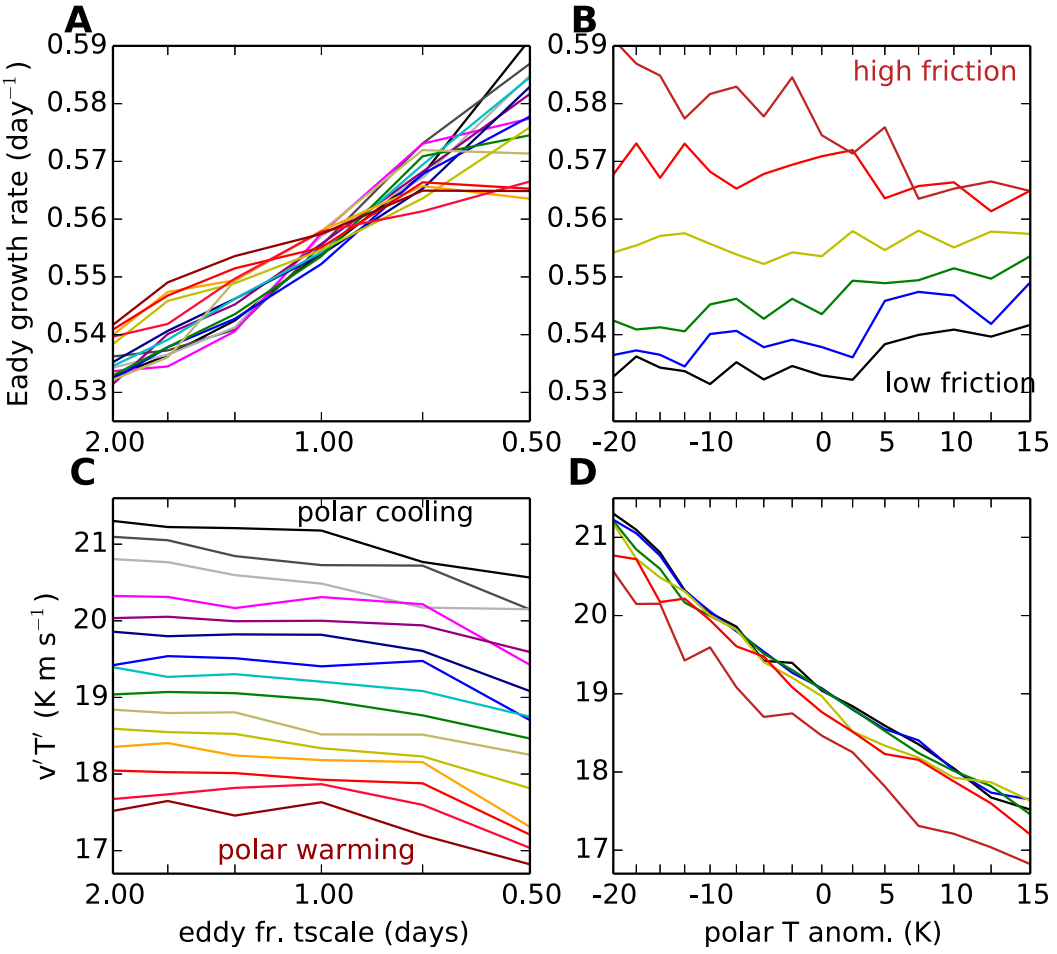

FIG. 5. (a),(b) Baroclinicity (at 775 hPa) and (c),(d) heat flux (at 850 hPa) for all experiments, both averaged in latitude over the mixing zone (see text for details). Each line in (a) and (c) marks experiments with the same thermal forcing, and each line in (b) and (d) marks experiments with the same eddy friction.

width of the baroclinic zone of the control run (defined as above), centered around the maxima in the heat flux of the forced runs. This method yields more robust results for a wide range of heat flux thresholds used to define the mixing zone.

The results in Fig. 5 show that the two-way equilibration predicted by the Ambaum–Novak model is evident. Baroclinicity and heat flux are proportional to the eddy friction and thermal forcing, respectively, with no strong relationships vice versa. These results are qualitatively similar for any reasonable heat flux percentage values used to define the baroclinic zone (e.g., zones defined using values of 30%–80% of heat flux maximum).

A closer inspection of the responses reveals that they are relatively small compared to the amount of thermal forcing or eddy friction applied. More specifically, for a factor-of-2 change in the equator–pole temperature gradient in the T_r field (i.e., the thermal forcing), the heat flux increases by about 15%. On the other hand, a factor-of-4 increase in eddy friction leads to a 10% increase in baroclinicity. However, a one-to-one relationship between the forcing/friction and the responses is not expected because of the inability to vary local advective processes externally (as discussed in the previous section) and, more importantly, because of the geographical restriction of the forcing/friction changes.

It is noted that stronger relationships between eddy friction and baroclinicity and diabatic forcing and eddy fluxes have been observed independently in channel models used by previous studies where such restrictions were not necessary (Zhang et al. 2012; Marshall et al. 2017). However, it is the relative response of baroclinicity and heat flux (in a more realistic atmosphere of a spherical GCM) that is of interest in the present study rather than the magnitude of the responses relative to the forcing/dissipation.

4. Mean available potential energy and eddy energy

The mean available potential energy (APE) can be viewed as the energy of the mean thermal state that can be converted into eddies, and its variability in the midlatitudes is primarily modulated by eddy activity (Novak and Tailleux 2018). In fact, in an idealized atmosphere with a constant horizontal temperature gradient, the quasigeostrophic (QG) form of APE [originally defined by Lorenz (1955)] is proportional to the square of the domain-integrated maximum Eady growth rate (Schneider 1981). Moreover, eddy energy (the sum of kinetic and available potential eddy energies) is a measure of eddy intensity. When diagnosed locally within the storm track, the mean APE and eddy energy may therefore be regarded as alternative measures of baroclinicity and storm-track activity, respectively. This section uses these measures and further tests the Ambaum–Novak model predictions.

Many studies use Lorenz's (1955) QG approximation to diagnose APE over the storm-track zone (e.g., O'Gorman and Schneider 2008; O'Gorman 2010). However, such local calculations are in fact approximate estimates because (i) they require the QG approximation and (ii) Lorenz's (1955) APE must be calculated over a domain with impermeable boundaries (i.e., the global domain) in order to be formally correct.

Instead of using Lorenz's (1955) classical definition of global APE, this analysis therefore uses a version that does not require the QG approximation and can be formally defined locally. Nevertheless, having repeated the analysis below for Lorenz's (1955) QG APE integrated over the baroclinic zone, it was found that both definitions yield qualitatively similar results.

The local APE was first introduced by Holliday and McIntyre (1981) and Andrews (1981) and recently adapted for diagnostic analysis in the atmosphere (Novak and Tailleux 2018). This local APE is essentially the vertical integral of the buoyancy forces between an actual state of the atmosphere and a reference state at rest (e.g., Holliday and McIntyre 1981; Andrews 1981). Following Novak and Tailleux (2018), the mean and eddy components of the local APE are defined as

$$\text{mean APE} = \overline{\int_{\tilde{p}_r}^{p} \alpha([\theta], p'') - \alpha\{\theta_r(p'', t), p''\}\, dp''}, \tag{6}$$

$$\text{eddy APE} = \overline{\left[\int_{p_r}^{\tilde{p}_r} \alpha(\theta, p'') - \alpha\{\theta_r(p'', t), p''\}\, dp''\right]}, \tag{7}$$

where α is the specific volume, θ is the potential temperature, θ_r the potential temperature of the reference state (which is, in this case, defined as the global area-weighted isobaric average of θ, equivalent to the reference state of Lorenz's APE), p is the pressure, and p_r and $\tilde{p}_r$ are the reference pressures defined as

$$\theta_r(p_r, t) = \theta \quad [\theta_r](\tilde{p}_r, t) = [\theta]. \tag{8}$$

The double prime denotes an integration variable. Again, the square brackets denote zonal mean, and the bar is the time mean. More information on the local APE can be found in Tailleux (2013) and Novak and Tailleux (2018). The results below are integrated over the depth of the troposphere (i.e., 1000–200 hPa) and averaged over the mixing zone.

The responses of the mean APE are very sensitive to the choice of the mixing zone. However, for some cases, such as most of the experiments in Figs. 6a and 6b (where the mixing zone was defined as the region where heat flux is within 55% of the maximum value), there is a correspondence with the responses of the baroclinicity, though the mean APE responses are somewhat weaker. For polar warming, the responses show less agreement, but this can be corrected (at the expense of the other runs) by slightly changing the threshold value to redefine the mixing zone. The high sensitivity to the choice of the mixing zone also applies to the Lorenz APE definition.

This sensitivity is caused by the mean APE exhibiting a minimum at the latitudes of the storm tracks (Fig. 7; thin black contours), which is a consequence of both APE definitions being defined to be proportional to the squared departures from a horizontally constant reference state of potential temperature. This makes its responses largely nonlocal (Fig. 7; colors), and if the responses are spatially complex as they are for the thermal forcing (Figs. 7c,d), then different signs of the responses can be obtained for slightly different heat flux thresholds used to define the mixing zone (e.g., 30% and 70%, both of which have been advocated by previous works). The mean APE is therefore not an ideal diagnostic for the equilibration of storm tracks. This is in contrast with the maximum Eady growth rate or the isentropic slope (below), both of which exhibit maxima in the center of storm tracks, and their responses are much less sensitive to the width of the mixing zone.

Eddy available potential and eddy kinetic energies (Figs. 6c–f) can be viewed as measures of storm-track activity, though one needs to be aware of the inclusion of barotropic waves in these terms. The eddy APE changes in accordance with the eddy heat flux, showing a consistent increase in the response to polar cooling and a weak sensitivity to eddy friction. The eddy kinetic energy exhibits a more complex behavior, but its baroclinic component (Figs. 6g,h), extracted as in Chen (1983), shows a very similar variability to that of the eddy APE and eddy heat flux. Because both eddy energies exhibit

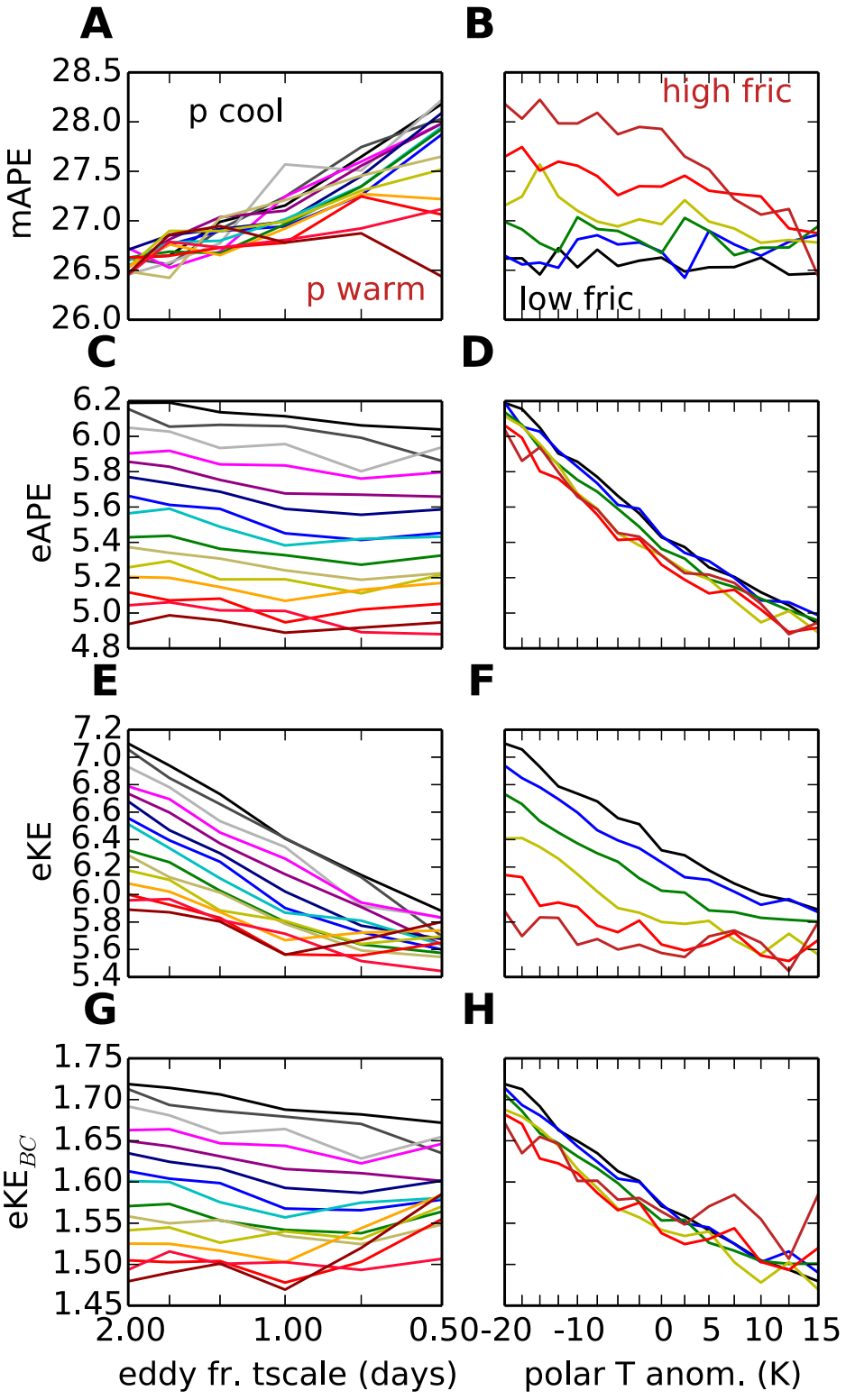

FIG. 6. As in Fig. 5, but for (a),(b) the local mean APE (integrated vertically and averaged over the baroclinic zone), (c),(d) global eddy APE, (e),(f) global eddy kinetic energy, and (g),(h) global baroclinic eddy kinetic energy. The global energy terms were computed as in Lorenz (1955), and the eddy kinetic energy was split into its baroclinic part as per Chen (1983). Units are 10^5 J m^{-2}.

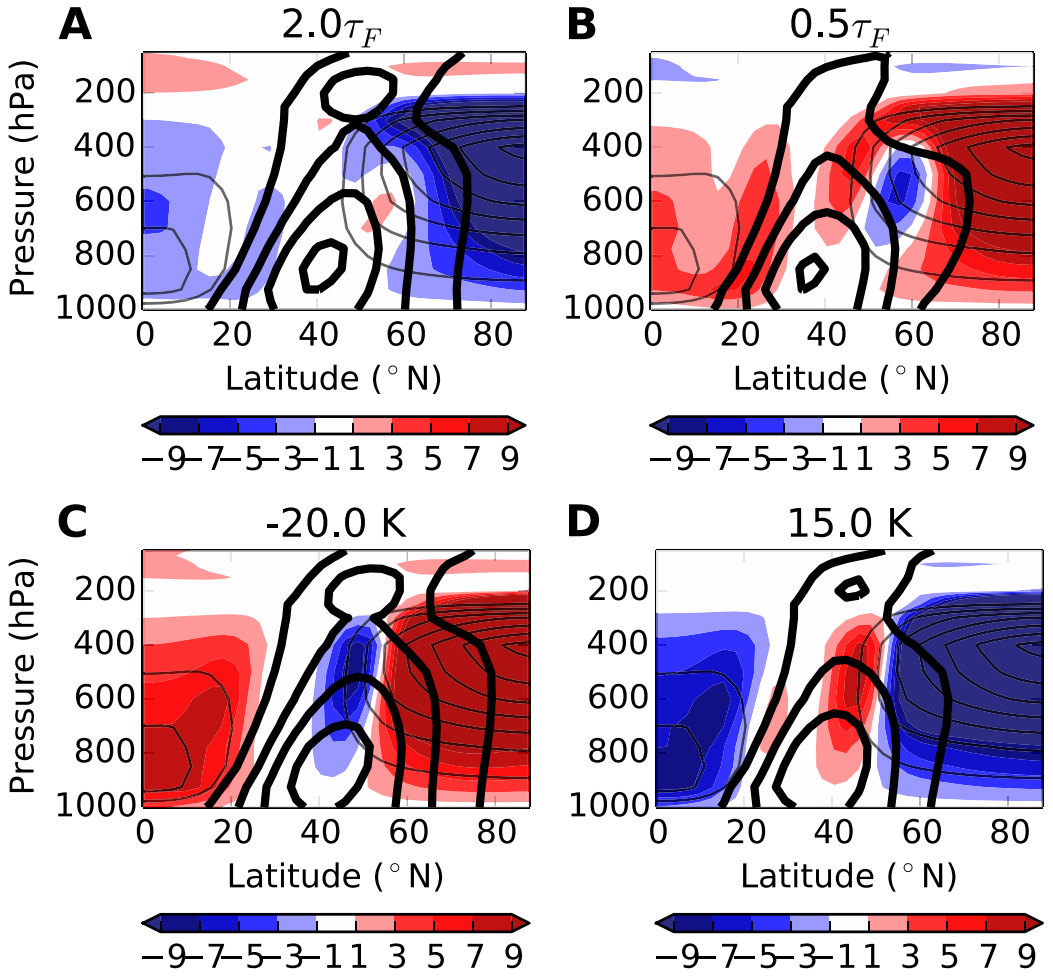

FIG. 7. Time-mean local APE [calculated using Eq. (6)] responses. The thin black contours show the absolute values of the control run (starting at 5×10^5 J kg^{-1} in the midlatitudes with intervals of 5×10^5 J kg^{-1}). The color shading shows the anomalies from the control run of the extreme cases of the reference runs, viz., showing the runs of (a) lowest and (b) highest eddy friction and the (c) highest and (d) lowest polar cooling. Units are 10^4 J kg^{-1}. The absolute values of the heat flux field are also shown in the thick black contours (starting at 5 K m s^{-1} with intervals of 5 K m s^{-1}).

maxima only within the mixing zone, these responses are robust for both local and global averages.

The energy responses generally concur with the predicted two-way equilibration but also reveal additional spatial complexity in the mean APE. This is due to its nonlocal definition and the confinement of the storm tracks to the midlatitudes. This complexity is obscured in the global Lorenz APE formulation, which may give a misleading picture of the APE responses within storm tracks.

5. Criticality

As in Schneider and Walker (2006), criticality is defined as

$$\xi = \frac{f}{\beta\left(p_0 - \overline{[p_t]}\right)} \frac{\overline{\partial_y[\theta]}}{\overline{\partial_p[\theta]}}, \tag{9}$$

where f is the Coriolis parameter, β its meridional derivative, p_0 the surface pressure, and p_t the pressure of the tropopause (estimated using the WMO definition as the lowermost point, where the lapse rate is equal to or lower than 2 K km^{-1}). Here, $\overline{\partial_y[\theta]}/\overline{\partial_p[\theta]}$ is the isentropic slope computed as the ratio of the meridional and vertical potential temperature (zonal and time mean) gradients in the low-level atmosphere. This section evaluates criticality (and related quantities) on the 850-hPa level.

Before analyzing the bulk value of criticality, it is insightful to examine the f/β ratio and the spatial structure

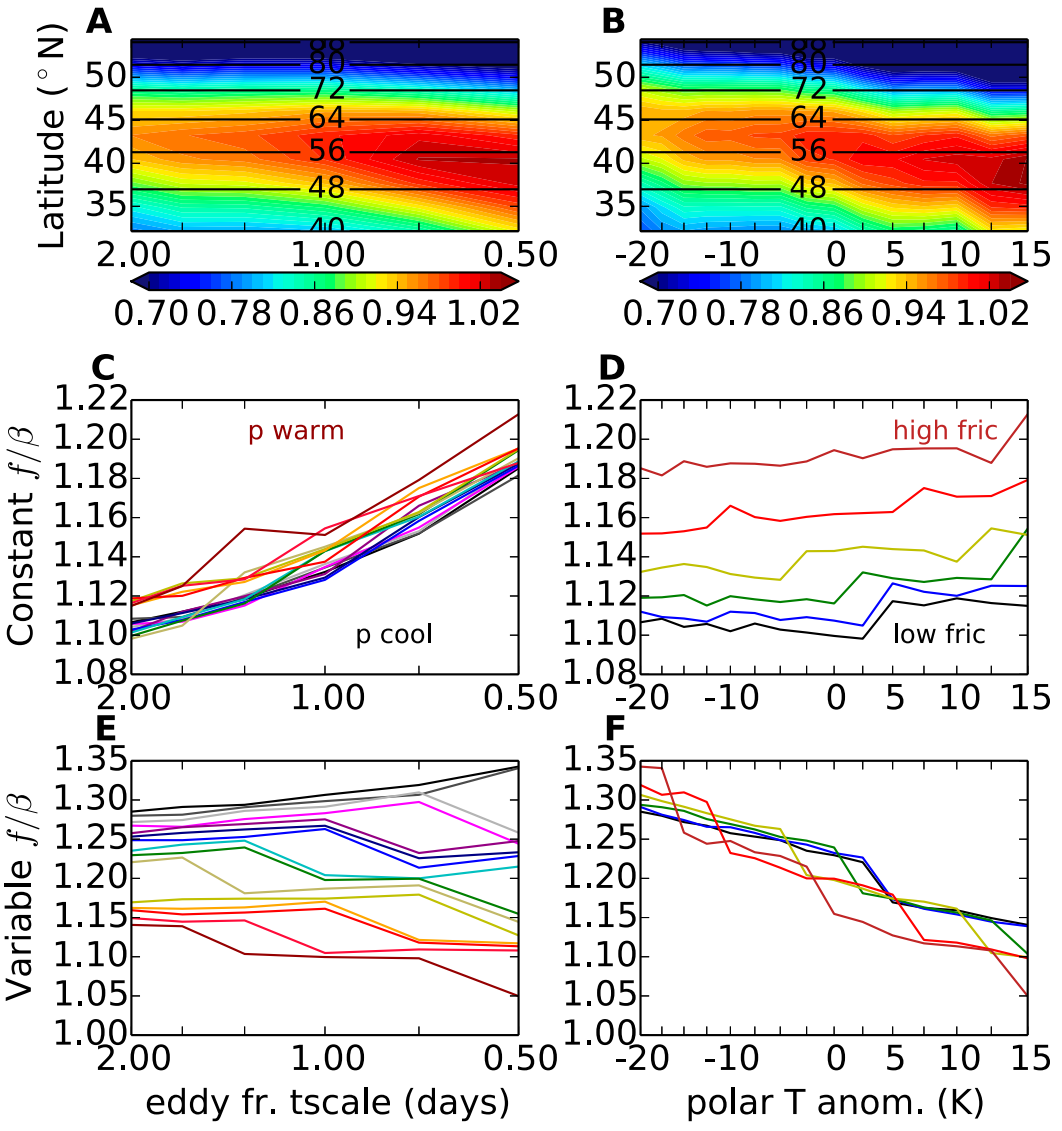

FIG. 8. Low-level dimensionless criticality response displayed as (a),(b) a scaled isentropic slope (colors) for the reference runs, (c),(d) the isentropic slope scaled with a variable tropopause height and constant f/β for all runs, and (e),(f) criticality using a variable tropopause height and variable f/β for all runs. The values in (c)–(f) are averaged over the baroclinic zone and computed on the 850-hPa level. Also displayed in (a) and (b) are the values of the f/β ratio (10^5 m).

of the isentropic slope ($\overline{\partial_y[\theta]}/\overline{\partial_p[\theta]}$) separately, as shown in Figs. 8a and 8b for the reference runs only. The isentropic gradient was scaled to have dimensions of criticality, using the average f/β ratio across the baroclinic zone of the control run, and $(p_0 - \overline{[p_t]})^{-1} = R\overline{[T]}/gp\overline{[H]}$, with g being the gravitational acceleration, R the gas constant for ideal gas, T the temperature, p the pressure, and H the height of the tropopause of the restoration temperature profile.

As with baroclinicity and local mean APE, eddy friction increases the isentropic slope. In the case of the thermal forcing, the eddy-induced static stability response overcompensates again for the response in the meridional temperature gradient. This results in a decrease in the isentropic slope of the actual state despite the imposed increase of the isentropic slope in the temperature restoration field [T_r in Eq. (3)]. This overcompensation appears to be stronger than for baroclinicity, because the isentropic slope has a stronger dependence on N.

Figures 8c and 8d show a summary of all responses in criticality, calculated using Eq. (9), again with a constant f/β ratio but with a varying tropopause height, and

averaged over the baroclinic zone as in the previous section. The responses follow those of the isentropic slope, with a slight overcompensation by static stability causing some reduction with polar cooling. It is also evident that varying tropopause height has negligible effect on the criticality.

The signs of the responses change dramatically if criticality is calculated using f/β that is computed at the mean latitude of the storm track, defined by Levine and Schneider (2015) as

$$\phi_M = \frac{\int_{\phi_{\rm EQ}}^{\phi_P} \overline{[v^*T^*]}\phi \, dy}{\int_{\phi_{\rm EQ}}^{\phi_P} \overline{[v^*T^*]} \, dy}, \tag{10}$$

where ϕ is the latitude, the square brackets denote zonal mean and the asterisks perturbations thereof and $\phi_{\rm EQ}$ and ϕ_P are the equatorward and poleward boundaries of the baroclinic zone, respectively. Criticality appears to be more responsive to the thermal forcing than the eddy friction (Figs. 8e,f).The steplike structure of changes in Figs. 8e and 8f is the result of the low resolution of the model setting. The changes in the storm-track latitude (ranging between 38° and 44°N) dominate the criticality response.

As opposed to the measures of eddy growth discussed above (i.e., baroclinicity, mean APE, and isentropic slope), the definition of criticality additionally includes β. If latitudinal shifts of the storm track occur, then the β effect dominates and causes criticality to decrease with a more equatorward position of the storm track. Green's (1960) study of analytical models of baroclinic instability suggests that the β effect mainly reflects changes in the eddy shape and size rather than changes in the eddy growth rate. This agrees with the apparent difference between the responses of criticality and the other measures of eddy growth. The other eddy growth measures are only weakly sensitive to the latitude of the storm track, and they generally concur with the Ambaum–Novak predictions.

6. Discussion and conclusions

It has been shown that the seemingly counterintuitive two-way equilibration of storm tracks to extratropical thermal forcing and eddy friction, as predicted by the Ambaum–Novak model, can be generally simulated in Earthlike model simulations. Eddies adjust to changes in the thermal forcing of the mean baroclinicity, and the mean baroclinicity adjusts to changes in the frictional dissipation of eddies.

The response to thermal forcing is equivalent to the generalized baroclinic adjustment of the atmosphere (Zurita-Gotor and Lindzen 2001; Zurita-Gotor 2007) and is reminiscent of the eddy saturation phenomenon in the Southern Ocean [as studied by Munday et al. (2013)]. Eddies act to maintain the flow near a point of baroclinic neutrality by limiting their own growth rate. They do this both by reducing the meridional temperature gradient and by increasing static stability via the horizontal and vertical heat fluxes, respectively. Even in quasigeostrophic atmospheric models with constant static stability, the eddy meridional heat flux is sufficient to keep the mean baroclinicity only weakly sensitive to the baroclinicity forcing (Zurita-Gotor and Vallis 2009). In the present GCM experiments, the strong responsiveness of eddies to increased thermal forcing is apparent in eddy heat flux, eddy APE, and baroclinic eddy kinetic energy.

In terms of the eddy friction–controlled equilibration, the maximum Eady growth rate, mean APE, and isentropic slope are all locally directly proportional to eddy dissipation, while the (baroclinic) eddy quantities are only weakly sensitive, as predicted. This relationship has not been previously shown unambiguously, and it is argued here that it is the flip side of the baroclinic adjustment phenomenon. These two relationships should be considered in tandem in the context of the equilibration of storm tracks. Both of these relationships have already been observed in simulations of the Southern Ocean, whereby oceanic eddies transfer their energy via form drag to the bottom of the ocean where the energy dissipates (Marshall et al. 2017).

However, the atmospheric GCM equilibration also includes characteristics that are not predicted by the Ambaum–Novak model. The midlatitude atmospheric response on a sphere is spatially complex [more than in the Marshall et al.'s (2017) channel model of the Southern Ocean] because of the latitudinally restricted extent of the midlatitude storm tracks. Beyond the storm tracks, the eddies are unable to modify the thermal structure of the atmosphere substantially, so care needs to be taken when interpreting variables (such as the mean APE), whose definitions depend on the global atmospheric state.

It should also be noted that changing the Newtonian cooling term in the GCM experiments [i.e., T_r in Eq. (3)] is not exactly equivalent to changing the constant diabatic forcing in the Ambaum–Novak model [i.e., F in Eq. (1)]. In addition, the Ambaum–Novak model is also unable to predict the GCM's overcompensation by static stability in response to thermal forcing, since the Ambaum–Novak model assumes a constant static stability. Quasigeostrophic scaling suggests that thermal forcing should affect the vertical heat fluxes more strongly than the meridional heat fluxes (Zurita-Gotor and Vallis 2009). In other words, even though the direct thermal forcing is to increase the mean meridional

temperature gradient (which is to a large extent reduced by horizontal eddy increased heat fluxes), the invigorated eddies also increase the mean static stability (by the their vertical heat fluxes). If the latter effect dominates, then the baroclinicity may be reduced (through the increased static stability) even though the direct thermal forcing was to increase it (by increasing the meridional temperature gradient). This overcompensation is apparent in the decreases in baroclinicity in some of the GCM experiments in this study and is more pronounced for the isentropic slope (which has a higher dependency on static stability than the maximum Eady growth rate or the mean APE). The strength of this overcompensation also decreases with increasing eddy friction.

There are also limitations of using the GCM to simulate the atmospheric storm tracks. First, Held–Suarez GCMs have additional nonlocal eddy dissipation through thermal relaxation because of the Newtonian cooling approximation. Moreover, Zhang and Stone (2011) have found that, for a coupled atmosphere–ocean system, boundary layer processes are determined by thermal damping, and the baroclinic adjustment can only be achieved in the free troposphere. The GCM in this study cannot reproduce these boundary layer processes that are more characteristic of the real atmosphere. Furthermore, moisture effects were neglected, and the associated latent heat release and cloud feedbacks are likely to alter the precise sensitivity of the equilibration (e.g., Hoskins and Valdes 1990; Voigt and Shaw 2015; Ceppi et al. 2017). It would therefore be insightful to repeat the above analysis in a more realistic coupled model.

As well as the limitations of the GCM, the fact that the Ambaum–Novak model lacks nonlinear barotropic interactions between eddies and the mean flow (e.g., wave breaking) and parameterizes all (direct and indirect) eddy effects into a single variable may be attributed to the smaller sensitivity of GCM responses relative to the predicted responses. Nevertheless, since other studies that used simpler channel models (e.g., Zhang et al. 2012; Marshall et al. 2017) were able to recover a much stronger dependence than the present results, it is more likely that this relatively small sensitivity is specific to using a GCM rather than being due to an inability of the Ambaum–Novak model to predict the fundamental equilibration.

It should be noted that the theoretical prediction of this two-way equilibration is not a unique feature of the Ambaum–Novak model. In fact, parallels can be drawn with both Lorenz's (1984) and Thompson's (1987) models, as discussed in Novak et al. (2017). In essence, both types of equilibration ensure that, in a steady state, the eddy dissipation rate matches the eddy growth rate (baroclinicity) and that the forcing of the baroclinicity matches the baroclinicity erosion by eddies. The presence of this two-way equilibration in theoretical models, as well as in atmospheric and oceanic GCMs, suggests that this is a general feature of baroclinically unstable systems.

In terms of the implications for the large-scale circulation, shifts in the overturning circulation and the associated midlatitude jet (as well as the eddy momentum fluxes—not shown) were found to be of a comparable magnitude for the thermal forcing and eddy friction despite the nonsymmetric responses in baroclinicity and baroclinic eddies. Although a detailed consideration of momentum exchanges in this two-way equilibration is the subject of a different study, the existence of the two-way equilibration indicates that the baroclinicity–eddy exchanges are the primary responses, concurring with the numerical solutions described in Hart (1979). Nevertheless, the responses of the momentum fluxes and the meridional overturning circulation are still an important factor that determines the three-dimensional properties of the baroclinic zone (e.g., Zurita-Gotor and Lindzen 2004; Blanco-Fuentes and Zurita-Gotor 2011; Nie et al. 2013).

The comparable shifts in the latitude of the eddy-driven circulation further demonstrate that such shifts are not linearly related to the storm-track activity (a causal link often used to explain jet shifts in climate models). This agrees with existing theories (e.g., Thorncroft et al. 1993; Orlanski 2003; Rivière 2009), which suggest that latitudinal jet shifts can be induced by changes in either baroclinicity (which can modulates the sign of the dominant momentum fluxes) or the strength of baroclinic eddies (because of their default preference to supply poleward momentum fluxes into the jet). The lack of symmetry of the two-way equilibration of baroclinicity and baroclinic eddies (and their independent ability to modify the mean flow) may help better to understand the uncertainty in the responses of the midlatitude storm tracks and the associated jets predicted by comprehensive climate models (Shepherd 2014). We are currently analyzing the combined biases in baroclinicity and heat fluxes in such climate models.

The rest of this section addresses the seemingly contradictory issues with previous literature outlined in the introduction. First, both the global-mean APE and eddy kinetic energy have been observed to increase with radiative forcing of storm tracks (O'Gorman and Schneider 2008; O'Gorman 2010), yet the Ambaum–Novak model predicts that the mean APE should be insensitive to this forcing (and storm-track activity). The mean APE responses have been found to be spatially complex and very sensitive to the choices used to define the baroclinic mixing zone over which the mean APE is averaged. For wide-enough mixing zones, a directly proportional relationship between the forcing and mean APE can be

found (though this relationship weakens for stronger eddy friction), which is broadly consistent with the previous studies. It is argued here that because of the nonlocal nature of its definition, APE is not a good diagnostic of storm-track equilibration. Nevertheless, it still agrees locally with the characteristics of the baroclinic adjustment and the dissipative control discussed above.

Second, Chen et al. (2007) have found a strong dependency of eddy kinetic energy to global eddy frictional dissipation. In the experiments presented here, this is true for the barotropic part of the eddy kinetic energy but not for the baroclinic component. The latter is proportional to eddy APE, both of which are only weakly and nonmonotonically sensitive to eddy friction (generally agreeing with the Ambaum–Novak predictions). Similarly, in the experiments of O'Gorman and Schneider (2008) mentioned above, the eddy kinetic energy is not divided into its barotropic and baroclinic parts, which may be responsible for the observed proportionality between the mean APE and eddy kinetic energy when responding to changes in radiative forcing. More insight may be gained by isolating the high-frequency transient eddies from planetary-scale Rossby waves, which have been found to have opposite effects on the mean flow (Hoskins et al. 1983).

To conclude, the two-way equilibration to thermal forcing and eddy friction predicted by purely baroclinic theory can be observed in primitive equations of atmospheric, as well as oceanic, GCMs. This equilibration is characterized by a strong response in eddy growth rate (measured by baroclinicity-like quantities) to eddy friction and a strong response in baroclinic eddy intensity to a mean temperature gradient forcing. The two-way equilibration is of relevance to climate modeling studies, where the circulation response to changes in the global radiation and eddy dissipative parameterizations is still not fully understood.

Acknowledgments. This work is supported by the U.K. Natural Environment Research Council (Grant NE/M014932/1), and we thank our reviewers for their very helpful feedback.

REFERENCES

Ambaum, M. H. P., and L. Novak, 2014: A nonlinear oscillator describing storm track variability. *Quart. J. Roy. Meteor. Soc.*, **140**, 2680–2684, https://doi.org/10.1002/qj.2352.

Andrews, D. G., 1981: A note on potential energy density in a stratified compressible fluid. *J. Fluid Mech.*, **107**, 227–236, https://doi.org/10.1017/S0022112081001754.

Blanco-Fuentes, J., and P. Zurita-Gotor, 2011: The driving of baroclinic anomalies at different timescales. *Geophys. Res. Lett.*, **38**, L23805, https://doi.org/10.1029/2011GL049785.

Ceppi, P., F. Brient, M. D. Zelinka, and D. L. Hartmann, 2017: Cloud feedback mechanisms and their representation in global climate models. *Wiley Interdiscip. Rev.: Climate Change*, **8**, e465, https://doi.org/10.1002/wcc.465.

Chen, G., I. M. Held, and W. A. Robinson, 2007: Sensitivity of the latitude of the surface westerlies to surface friction. *J. Atmos. Sci.*, **64**, 2899–2915, https://doi.org/10.1175/JAS3995.1.

Chen, T.-C., 1983: The energy exchange between the baroclinic and barotropic components of atmospheric flow in the tropics during the FGGE summer. *Mon. Wea. Rev.*, **111**, 1389–1396, https://doi.org/10.1175/1520-0493(1983)111<1389:TEEBTB>2.0.CO;2.

Fraedrich, K., E. Kirk, and F. Lunkeit, 1998: PUMA: Portable University Model of the Atmosphere. Deutsches Klimarechenzentrum Tech. Rep. 16, 38 pp.

——, ——, U. Luksch, and F. Lunkeit, 2005: The Portable University Model of the Atmosphere (PUMA): Storm track dynamics and low-frequency variability. *Meteor. Z.*, **14**, 735–745, https://doi.org/10.1127/0941-2948/2005/0074.

Green, J. S. A., 1960: A problem in baroclinic stability. *Quart. J. Roy. Meteor. Soc.*, **86**, 237–251, https://doi.org/10.1002/qj.49708636813.

Hart, J. E., 1979: Finite amplitude baroclinic instability. *Annu. Rev. Fluid Mech.*, **11**, 147–172, https://doi.org/10.1146/annurev.fl.11.010179.001051.

Harvey, B., L. Shaffrey, and T. Woollings, 2013: Equator-to-pole temperature differences and the extra-tropical storm track responses of the CMIP5 climate models. *Climate Dyn.*, **33**, 1171–1182, https://doi.org/10.1007/s00382-013-1883-9.

Held, I. M., and M. J. Suarez, 1994: A proposal for the intercomparison of the dynamical cores of atmospheric general circulation models. *Bull. Amer. Meteor. Soc.*, **75**, 1825–1830, https://doi.org/10.1175/1520-0477(1994)075<1825:APFTIO>2.0.CO;2.

Holliday, D., and M. E. McIntyre, 1981: On potential energy density in an incompressible stratified fluid. *J. Fluid Mech.*, **107**, 221–225, https://doi.org/10.1017/S0022112081001742.

Hoskins, B. J., and A. J. Simmons, 1975: A multi-layer spectral model and the semi-implicit method. *Quart. J. Roy. Meteor. Soc.*, **101**, 637–655, https://doi.org/10.1002/qj.49710142918.

——, and P. J. Valdes, 1990: On the existence of storm-tracks. *J. Atmos. Sci.*, **47**, 1854–1864, https://doi.org/10.1175/1520-0469(1990)047<1854:OTEOST>2.0.CO;2.

——, and K. I. Hodges, 2005: A new perspective on Southern Hemisphere storm tracks. *J. Climate*, **18**, 4108–4129, https://doi.org/10.1175/JCLI3570.1.

——, I. James, and G. White, 1983: The shape, propagation and mean-flow interaction of large-scale weather systems. *J. Atmos. Sci.*, **40**, 1595–1612, https://doi.org/10.1175/1520-0469(1983)040<1595:TSPAMF>2.0.CO;2.

James, I. N., 1994: *Introduction to Circulating Atmospheres.* Cambridge University Press, 230 pp.

Jansen, M., and R. Ferrari, 2012: Macroturbulent equilibration in a thermally forced primitive equation system. *J. Atmos. Sci.*, **69**, 695–713, https://doi.org/10.1175/JAS-D-11-041.1.

——, and ——, 2013: Equilibration of an atmosphere by adiabatic eddy fluxes. *J. Atmos. Sci.*, **70**, 2948–2962, https://doi.org/10.1175/JAS-D-13-013.1.

Kållberg, P., P. Berrisford, B. Hoskins, A. Simmmons, S. Uppala, S. Lamy-Thépaut, and R. Hine, 2005: ERA-40 atlas. ECMWF ERA-40 Project Rep. 19, 191 pp.

Kim, H. K., and S. Lee, 2001: Hadley cell dynamics in a primitive equation model. Part II: Nonaxisymmetric flow. *J. Atmos. Sci.*, **58**, 2859–2871, https://doi.org/10.1175/1520-0469(2001)058<2859:HCDIAP>2.0.CO;2.

Levine, X. J., and T. Schneider, 2015: Baroclinic eddies and the extent of the Hadley circulation: An idealized GCM study. *J. Atmos. Sci.*, **72**, 2744–2761, https://doi.org/10.1175/JAS-D-14-0152.1.

Lorenz, E. N., 1955: Available potential energy and the maintenance of the general circulation. *Tellus*, **7**, 157–167, https://doi.org/10.3402/tellusa.v7i2.8796.

——, 1984: Irregularity: A fundamental property of the atmosphere. *Tellus*, **36A**, 98–110, https://doi.org/10.1111/j.1600-0870.1984.tb00230.x.

Marshall, D. P., M. H. P. Ambaum, J. R. Maddison, D. Munday, and L. Novak, 2017: Eddy saturation and frictional control of the Antarctic Circumpolar Current. *Geophys. Res. Lett.*, **44**, 286–292, https://doi.org/10.1002/2016GL071702.

Mbengue, C., and T. Schneider, 2013: Storm track shifts under climate change: What can be learned from large-scale dry dynamics. *J. Climate*, **26**, 9923–9930, https://doi.org/10.1175/JCLI-D-13-00404.1.

——, and ——, 2018: Linking Hadley circulation and storm tracks in a conceptual model of the atmospheric energy balance. *J. Atmos. Sci.*, **75**, 841–856, https://doi.org/10.1175/JAS-D-17-0098.1.

Munday, D. R., H. L. Johnson, and D. P. Marshall, 2013: Eddy saturation of equilibrated circumpolar currents. *J. Phys. Oceanogr.*, **43**, 507–532, https://doi.org/10.1175/JPO-D-12-095.1.

Nie, Y., Y. Zhang, X.-Q. Yang, and G. Chen, 2013: Baroclinic anomalies associated with the Southern Hemisphere annular mode: Roles of synoptic and low-frequency eddies. *Geophys. Res. Lett.*, **40**, 2361–2366, https://doi.org/10.1002/grl.50396.

Novak, L., and R. Tailleux, 2018: On the local view of atmospheric available potential energy. *J. Atmos. Sci.*, **75**, 1891–1907, https://doi.org/10.1175/JAS-D-17-0330.1.

——, M. H. P. Ambaum, and R. Tailleux, 2015: The lifecycle of the North Atlantic storm track. *J. Atmos. Sci.*, **72**, 821–833, https://doi.org/10.1175/JAS-D-14-0082.1.

——, ——, and ——, 2017: Marginal stability and predator–prey behaviour within storm tracks. *Quart. J. Roy. Meteor. Soc.*, **143**, 1421–1433, https://doi.org/10.1002/qj.3014.

O'Gorman, P. A., 2010: Understanding the varied response of the extratropical storm tracks to climate change. *Proc. Natl. Acad. Sci. USA*, **107**, 19 176–19 180, https://doi.org/10.1073/pnas.1011547107.

——, and T. Schneider, 2007: Recovery of atmospheric flow statistics in a general circulation model without nonlinear eddy-eddy interactions. *Geophys. Res. Lett.*, **34**, L22801, https://doi.org/10.1029/2007GL031779.

——, and ——, 2008: Energy of midlatitude transient eddies in idealized simulations of changed climates. *J. Climate*, **21**, 5797–5806, https://doi.org/10.1175/2008JCLI2099.1.

Oort, A. H., 1964: On estimates of the atmospheric energy cycle. *Mon. Wea. Rev.*, **92**, 483–493, https://doi.org/10.1175/1520-0493(1964)092<0483:OEOTAE>2.3.CO;2.

Orlanski, I., 2003: Bifurcation in eddy life cycles: Implications for storm track variability. *J. Atmos. Sci.*, **60**, 993–1023, https://doi.org/10.1175/1520-0469(2003)60<993:BIELCI>2.0.CO;2.

Pedlosky, J., 1992: *Geophysical Fluid Dynamics.* Springer, 230 pp.

Pithan, F., T. G. Shepherd, G. Zappa, and I. Sandu, 2016: Climate model biases in jet streams, blocking and storm tracks resulting from missing orographic drag. *Geophys. Res. Lett.*, **43**, 7231–7240, https://doi.org/10.1002/2016GL069551.

Polichtchouk, I., and T. G. Shepherd, 2016: Zonal-mean circulation response to reduced air–sea momentum roughness. *Quart. J. Roy. Meteor. Soc.*, **142**, 2611–2622, https://doi.org/10.1002/qj.2850.

Rivière, G., 2009: Effect of latitudinal variations in low-level baroclinicity on eddy life cycles and upper-tropospheric wave-breaking processes. *J. Atmos. Sci.*, **66**, 1569–1592, https://doi.org/10.1175/2008JAS2919.1.

Schneider, E. K., 1981: On the amplitudes reached by baroclinically unstable disturbances. *J. Atmos. Sci.*, **38**, 2142–2149, https://doi.org/10.1175/1520-0469(1981)038<2142:OTARBB>2.0.CO;2.

Schneider, T., and C. C. Walker, 2006: Self-organization of atmospheric macroturbulence into critical states of weak nonlinear eddy–eddy interactions. *J. Atmos. Sci.*, **63**, 1569–1586, https://doi.org/10.1175/JAS3699.1.

——, and ——, 2008: Scaling laws and regime transitions of macroturbulence in dry atmospheres. *J. Atmos. Sci.*, **65**, 2153–2173, https://doi.org/10.1175/2007JAS2616.1.

Shepherd, T. G., 2014: Atmospheric circulation as a source of uncertainty in climate change projections. *Nat. Geosci.*, **7**, 703–708, https://doi.org/10.1038/ngeo2253.

Stone, P. H., 1978: Baroclinic adjustment. *J. Atmos. Sci.*, **35**, 561–571, https://doi.org/10.1175/1520-0469(1978)035<0561:BA>2.0.CO;2.

Tailleux, R., 2013: Available potential energy density for a multicomponent Boussinesq fluid with arbitrary nonlinear equation of state. *J. Fluid Mech.*, **735**, 499–518, https://doi.org/10.1017/jfm.2013.509.

Thompson, P. D., 1987: Large-scale dynamical response to differential heating: Statistical equilibrium states and amplitude vacillation. *J. Atmos. Sci.*, **44**, 1237–1248, https://doi.org/10.1175/1520-0469(1987)044<1237:LSDRTD>2.0.CO;2.

Thorncroft, C. D., B. J. Hoskins, and M. E. McIntyre, 1993: Two paradigms of baroclinic wave life-cycle behaviour. *Quart. J. Roy. Meteor. Soc.*, **119**, 17–55, https://doi.org/10.1002/qj.49711950903.

Voigt, A., and T. A. Shaw, 2015: Circulation response to warming shaped by radiative changes of clouds and water vapour. *Nat. Geosci.*, **8**, 102–106, https://doi.org/10.1038/ngeo2345.

Zappa, G., G. Masato, L. Shaffrey, T. Woollings, and K. Hodges, 2014: Linking Northern Hemisphere blocking and storm track biases in the CMIP5 climate models. *Geophys. Res. Lett.*, **41**, 135–139, https://doi.org/10.1002/2013GL058480.

——, M. K. Hawcroft, L. Shaffrey, E. Black, and D. J. Brayshaw, 2015: Extratropical cyclones and the projected decline of winter Mediterranean precipitation in the CMIP5 models. *Climate Dyn.*, **45**, 1727–1738, https://doi.org/10.1007/s00382-014-2426-8.

Zhang, Y., and P. H. Stone, 2011: Baroclinic adjustment in an atmosphere–ocean thermally coupled model: The role of the boundary layer processes. *J. Atmos. Sci.*, **68**, 2710–2730, https://doi.org/10.1175/JAS-D-11-078.1.

——, X.-Q. Yang, Y. Nie, and G. Chen, 2012: Annular mode–like variation in a multilayer quasigeostrophic model. *J. Atmos. Sci.*, **69**, 2940–2958, https://doi.org/10.1175/JAS-D-11-0214.1.

Zurita-Gotor, P., 2007: The relation between baroclinic adjustment and turbulent diffusion in the two-layer model. *J. Atmos. Sci.*, **64**, 1284–1300, https://doi.org/10.1175/JAS3886.1.

——, and R. S. Lindzen, 2001: The equilibration of short Charney waves: Implications for potential vorticity homogenization in the extratropical troposphere. *J. Atmos. Sci.*, **58**, 3443–3462, https://doi.org/10.1175/1520-0469(2001)058<3443:TEOSCW>2.0.CO;2.

——, and ——, 2004: Baroclinic equilibration and the maintenance of the momentum balance. Part II: 3D results. *J. Atmos. Sci.*, **61**, 1483–1499, https://doi.org/10.1175/1520-0469(2004)061<1483:BEATMO>2.0.CO;2.

——, and G. K. Vallis, 2009: Equilibration of baroclinic turbulence in primitive equations and quasigeostrophic models. *J. Atmos. Sci.*, **66**, 837–863, https://doi.org/10.1175/2008JAS2848.1.